ACS OMEGA

http://pubs.acs.org/journal/acsodf Article

Coupling Supramolecular Assemblies and Reactive Oxygen Species (ROS) with Megasonic Action for Applications in Shallow Trench Isolation (STI) Post-Chemical Mechanical Planarization (p-CMP) Cleaning

Katherine M. Wortman-Otto, Don Watson, Don Dussault, and Jason J. Keleher*

Cite This: ACS Omega 2022, 7, 26029−26039

Read Online

ACCESS | Metrics & More | Article Recommendations

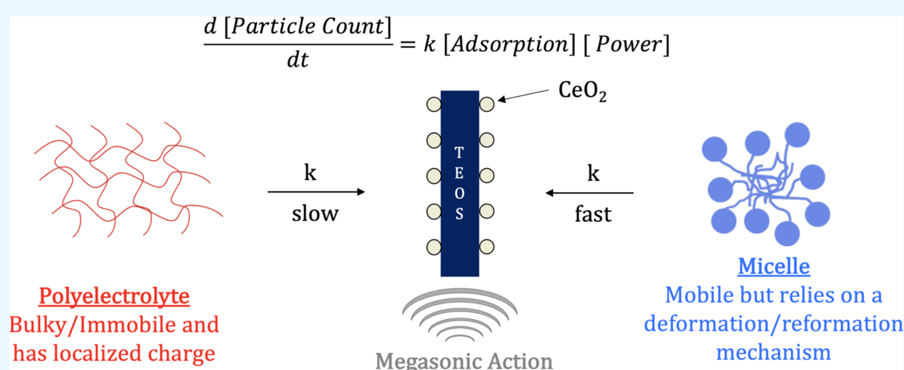

ABSTRACT: Due to the continued miniaturization of semiconductor devices, slurry formulations utilized in the chemical mechanical planarization (CMP) process have become increasingly complex to meet stringent manufacturing specifications. Traditionally, in shallow trench isolation (STI), CMP, a contact cleaning method involving a poly(vinyl alcohol) (PVA) brush, is used to effectively transfer cleaning chemistry to the oxide substrate. This PVA brush can cause nonuniform cleaning chemistry transport, increased interfacial shear force, and cleaning-induced defectivity from brush loading. Previous work with traditional cleaning processes has shown that using "soft" supramolecular cleaning chemistries has dramatically improved cleaning efficacy while also minimizing the number of induced p-CMP defects. To minimize these effects, noncontact cleaning via the implementation of megasonic action has gained attention. This work employs "soft" cleaning chemistries with Cu^{2+}−amino acid complexes, which can catalyze the formation of critical reactive oxygen species (ROS), and evaluates the p-CMP performance under megasonic action. Results from a second-order kinetic model indicate that megasonic conditions (i.e., time and power), "soft" cleaning chemistry structure (i.e., shape and charge), and the generation of ROS all play a critical role in cleaning efficacy under low shear stress conditions.

1. INTRODUCTION

With device feature size and complexity continuing to approach the 3 nm node, limiting induced defectivity during not only the polishing process but also the post-chemical mechanical planarization (p-CMP) process is of utmost importance.[1−6] To effectively achieve this, an understanding of the interactions between the slurry residue and cleaning formulations at the molecular level is crucial. Traditional p-CMP processes for STI involve a contact method of cleaning through PVA brush scrubbing.[7−9] This contact method has been coupled with different cleaning chemistry types, such as redox additives and surfactants, to effectively remove residual CeO_2 nanoparticles on the surface.[10,11] It has been widely accepted that the particle left on the TEOS wafer post-polish is predominantly Ce^{3+} as the presence of surface oxygen vacancies is critical during the polishing step.[4,12−16] This strong noncovalent interaction between the CeO_2 nanoparticle and wafer surface means that the cleaning chemistries used in the p-CMP process require a redox-active cleaning environment so that the particle can be removed via the charge flipping mechanism (i.e., converting Ce^{3+} to Ce^{4+}). While this has shown to be an effective mode of particle removal, there is an increase in the process shear force

Received: February 2, 2022
Accepted: May 20, 2022
Published: July 21, 2022

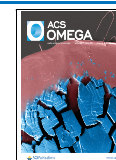

ACS Publications

© 2022 The Authors. Published by American Chemical Society

https://doi.org/10.1021/acsomega.2c00683
ACS Omega 2022, 7, 26029−26039

(mechanical component), which results in secondary defect formation (i.e., increased scratching/surface roughness).[17,18] More recently attention has shifted to developing p-CMP cleaning formulations that employ encapsulation of the CeO_2 nanoparticle using supramolecular chemistries (i.e., surfactants, polyelectrolytes, liposomes, etc.). Previous work has shown that the shape and charge of the supramolecular structure play a crucial role in effective CeO_2 nanoparticle removal.[19−21] More specifically, upon delivery to the wafer surface, micelles recover at a slower rate than polyelectrolytes. Though these additives do reduce the overall shear force and help to minimize defectivity induced during the cleaning process, it is not perfect and can cause p-CMP defects from the contact modality.

To minimize the aforementioned induced defectivity during contact p-CMP processes, the implementation of noncontact modalities has become of the utmost importance. The implementation of megasonic cleaning has gained attention as it utilizes acoustic cavitation to remove defects (i.e., nanoparticles and organic residue) from the wafer surface.[22−25] This method of cleaning applies an acoustic field to a liquid and in turn disrupts the liquid pressure and produces cavitation.[26−28] By adjusting the megasonic frequencies, the size and growth of the bubbles can be controlled. This cavitation can not only help remove particle and residue defects from the surface but it can also replenish the cleaning chemistry that gets to the surface. In addition to its noncontact modality, megasonic cleaning is beneficial for shrinking device nodes as its ability to reduce the boundary layer allows for the effective removal of submicron nanoparticles. To date, a majority of the cleaning chemistries used in megasonic cleaning have been redox chemistries that relied on the charge flipping mechanism (i.e., Ce^{4+} to Ce^{3+}) and nonionic surfactants to remove particles from the surface.[29,30]

This work focuses on implementing previously reported supramolecular cleaning chemistries to better understand the "soft" encapsulation mechanism of contaminant removal for noncontact cleaning modalities. More specifically, the work investigates changes in the equilibrium dynamics of supramolecular structure (i.e., micelle, polyelectrolyte, vesicle) formation/deformation impact on contaminant removal at the microscopic level under varying megasonic conditions. A structure function relationship will be developed using a second-order kinetic model to describe the cleaning efficiency. Additionally, the synergy between reactive oxygen species (ROS) generated during the megasonic process and the supramolecular structures employed in cleaning will be evaluated. Correlation of cleaning performance (i.e., nanoparticle removal) to the critical adsorption mechanism will be highlighted for the proposed soft p-CMP cleaning process.

2. MATERIALS AND METHODS

2.1. Exaggerated Wafer Surface Preparation. Exaggerated nanoparticle deposition conditions were simulated by coating 2.54 cm × 2.54 cm TEOS wafers (Advantiv Tech., Inc.) in a 1.0 wt % CeO_2 nanoparticle dispersion at pH 4 (provided by Ferro Corporation). This exaggeration was done to mimic worst-case scenario conditions. All wafers were dip-rinsed in pH 4 DI water to remove loosely bound particles.

2.2. Brush Cleaning Method. CeO_2-coated wafers were placed but not submerged in a 40 mL bath of a 0.1 wt % cleaning agent under a rotating PVA brush (Planarcore PVP1ARXR1) at 50 rpm for 1 min. The four cleaning agents studied in this work represent micelles, polyelectrolytes, and vesicles: 0.1 wt % Pluronic P-103 (BASF) as a nonionic micelle, 0.1 wt % Surfonic PE-1198LA (Hunstman) as a branched anionic micelle, 0.1 wt % poly-sorbate 20 (i.e., Tween 20) (Sigma-Aldrich) as a nonionic vesicle, and 0.1 wt % poly(4-styrene sulfonate, ammonium salt) (PSSA) (29.52% solids in water, ∼120,000 MW from Scientific Polymer Products, Inc.) as an anionic polyelectrolyte. The pH of the cleaning solutions was kept constant at 4.0. Additionally, all micelles and polyelectrolyte networks were formulated at 0.1 wt % as this is well above their respective CMC and aggregation threshold. It should be noted this concentration ensures homogeneity in the dispersion of the supramolecular structure.

2.3. Megasonic Cleaning Method. TEOS wafers, 2.54 cm × 2.54 cm, were prepared in exaggerated conditions in the same manner as previously mentioned for brush cleaning. Wafers were fully submerged vertically in 200 mL of the cleaning solution within the megasonic cleaning module (BowlMeg, ProSys Inc.). For the supramolecular chemistry only case, the same structures and working concentrations from the brush cleaning were utilized. The cleaning chemistry formulations used to generate ROS species were comprised of 90 μM $CuSO_4$ (98%, Alfa Aesar), 10 mM amino acid, 0.1 wt % of the previously mentioned supramolecular cleaning chemistries, and 0.1 wt % H_2O_2 (30 wt %, JT Baker). The amino acids used in this study were L-serine (≥99%, Sigma-Aldrich) and L-arginine (≥99%, Sigma-Aldrich). The order of addition for these ROS-generating cleaning chemistries is crucial. First, the organometallic complex is induced, the supramolecular cleaning chemistry is added, and finally, the oxidizer is incorporated. The megasonic cleaning parameters for time and power were controlled and ranged from 60 to 600 s and 0.5−1.5 W/cm^2, respectively. After cleaning the wafers in the megasonic cleaner with the desired chemistries, the wafers were then placed in a dehydrator for 5 min to expedite the drying process before measuring the particle count.

2.4. Particle Count: Dark-Field Fluorescence Spectroscopy. Dark-field fluorescence microscopy was utilized to effectively measure particle count on the post-cleaned 2.54 cm × 2.54 cm TEOS substrate. The cleaned wafers (method listed previously) were first treated with 1 μM sulforhodamine B (75%, Millipore Sigma) to tag the unremoved CeO_2 defects. The wafer was then rinsed with pH 4 DI H_2O to remove excess dye. The treated wafer was then exposed to a 532 nm light source to illuminate the sample directly. The fluoresced light then traveled through an objective lens (10×), a 550 nm bandpass filter, and a dichroic mirror before being captured by an Amscope MU6433-FL camera. Particle contaminants or scratches could be determined by fluctuations in the post-cleaned fluorescent images. These images were analyzed via ImageJ software (open source, National Institute of Health), where particle count measurements were determined. It must be noted that this technique has a limit of detection of 19 nm CeO_2 particles on the TEOS substrate. The authors acknowledge that there could be additional CeO_2 residues below the 50 nm threshold; however, this technique was used to monitor relative differences in the post-CMP performance.

2.5. Hydroxyl Radical ($^•$OH) Trapping. The concentration of $^•$OH generated was determined using a widely accepted methodology, which uses UV−vis spectroscopy and *p*-nitrosodimethylanline (PNDA) as a probe molecule.[31] The peak intensity of PNDA (97%, Sigma-Aldrich) occurs at 440 nm, and when the PNDA reacts with $^•$OH generated in the system, the peak intensity decreases. This well-known method was modified to track the generation of ROS species with the cleaning chemistries used in this study. PNDA was incorporated into the cleaning chemistry prior to the addition of the oxidizer. An

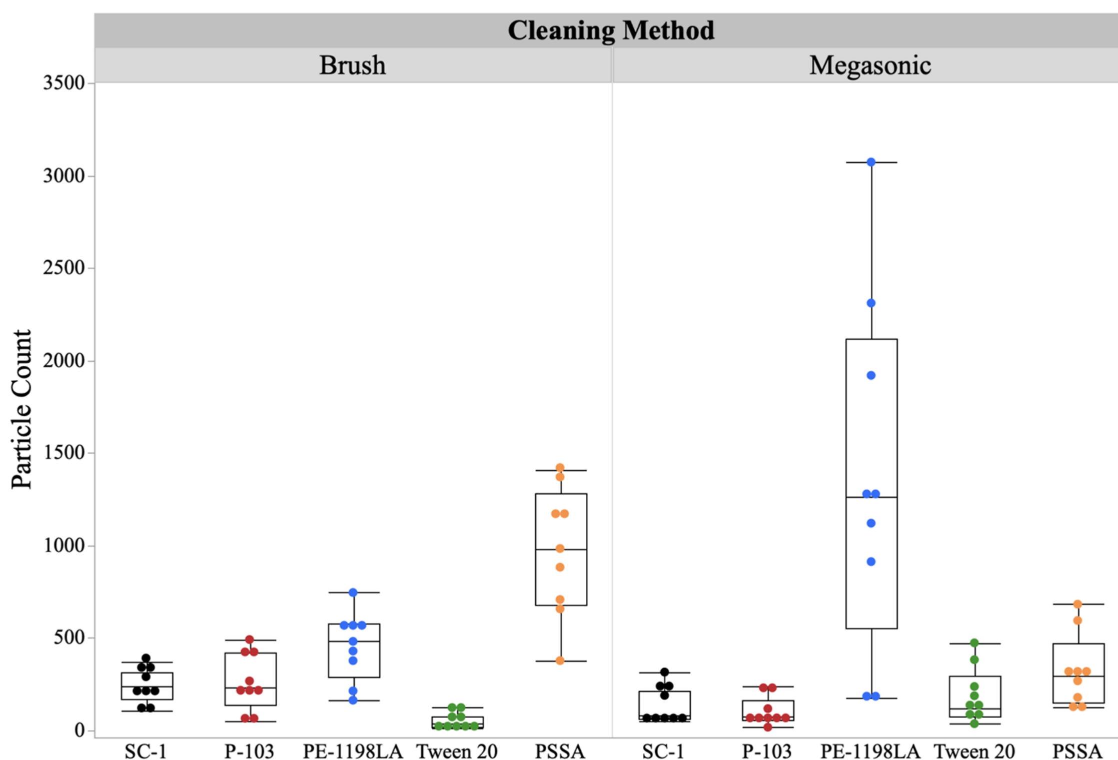

Figure 1. Supramolecular cleaning chemistry effect on particle count for brush and megasonic cleaning modes.

aliquot was taken and measured every 5 min for the duration of 1 h using a Persee T7S UV−vis spectrometer. To look at the effect of physical conditions on the generation of •OH, static (no mixing), dynamic (mixed with a paddle mixer), and megasonic (megasonic cleaning at 0.5 W/cm^2) cleaning were run.

2.6. Modified Quartz Crystal Microbalance (QCM) Technique. A Gamry eQCM 10 MTM QCM was utilized to track changes in crystal frequency upon the addition of cleaning chemistry. The 5 MHz Au Quartz Crystal Wrap-around Electrode (Renlux Crystal) used was modified by casting a thin film of CeO_2 to represent the particle remaining on the wafer surface. This film was deposited by casting a solution of 0.1 wt % CeO_2 in ethanol on the electrode surface. Then, 7 mL of the 0.1 wt % cleaning agents was injected into the sample holder to track changes in the crystal frequency. The changes in the frequency could then be correlated to subtle changes in mass (i.e., adsorption/desorption) through the Sauerbrey equation. For this experiment, the sample was monitored for 2 s post-injection to look at the initial interaction between the simulated wafer surface and the supramolecular cleaning chemistries.

3. RESULTS AND DISCUSSION

Though traditional brush cleaning can be effective in removing nanoparticles from the wafer surface, this removal mechanism has shown to also induce further defectivity. This increase in wafer defectivity can be attributed to the uptake of polish waste (i.e., slurry, pad, organic residue, etc.) into the brush matrix, which under contact modality results in further defect formation (i.e., waste redeposition and scratching). To limit this induced defectivity, the supramolecular cleaning chemistries were utilized in a noncontact mode (i.e., static megasonic tank) to evaluate their p-CMP performance. Figure 1 is a summary of exaggerated condition particle counts comparing contact (brush) and noncontact (megasonic) modes of cleaning with supramolecular chemistries.

Under the exaggerated methods, contact and noncontact cleaning seem to show similar particle removal performance with the supramolecular cleaning chemistries. In the case of SC-1, the industry standard, both modalities allow for the surface reactivity and charge flipping required. Though the particle count is low, SC-1 can induce further defectivity due to its strong undercutting and surface modification, leading to increased scratch counts. When looking at the traditional brush cleaning compared to megasonic cleaning in the presence of supramolecular chemistries, the variability of the megasonic is significantly lower, which indicates an enhanced interaction with the wafer surface. The only exception to this finding is the branched anionic micelle (PE-1198LA), which shows a significant increase in variability with megasonic cleaning. This could be due to the breakdown of the anionic micelle structure wherein the monounit bulkiness of the two-tailed system prevents effective interaction at the surface. Furthermore, the anionic nature of the head allows for the adsorption to the residual CeO_2 particle at the wafer surface but does not allow for its subsequent removal. The mode of nanoparticle removal is directly related to the effective delivery of the chemistry to the wafer surface. Without effective delivery of the supramolecular structure to the wafer surface, the necessary particle encapsulation is hindered resulting in an unproductive removal mechanism.

The rate of particle removal for this work is impacted by two (second-order kinetic model) key contributing factors: (1) the power of the megasonic cleaning (0.5−1.5 W/cm^2) and (2) the transport of the supramolecular cleaning chemistries to the wafer surface, as represented by eq 1.

https://doi.org/10.1021/acsomega.2c00683
ACS Omega 2022, 7, 26029−26039

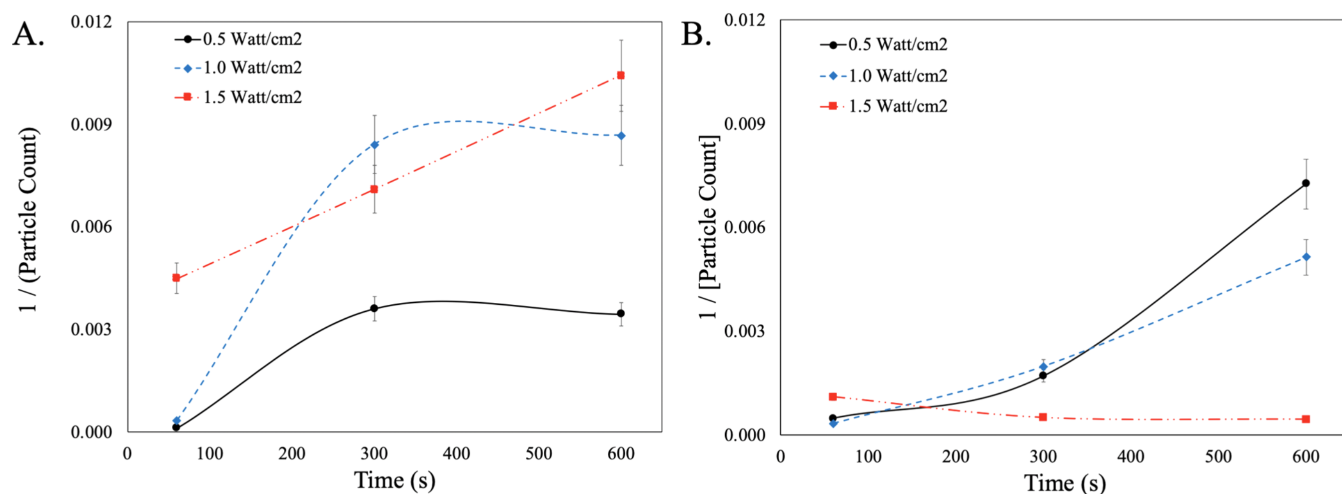

Figure 2. Second-order kinetic analysis of particle count for SC-1 cleaning. (A) Continuous megasonic wave and (B) pulsed-wave megasonic conditions.

Figure 3. Evaluation of cleaning performance for supramolecular cleaning chemistries using a second-order kinetic model for continuous wave megasonic conditions. (A) PE-1198LA, (B) P-103, (C) PSSA, and (D) Tween 20.

$$\frac{\mathrm{d}[\text{particle count}]}{\mathrm{d}t} = k[\text{adsorption}]\,[\text{megasonic power}] \quad (1)$$

The above relationship was selected as it connects the solution chemistry transport (i.e., surfactants and ROS) to the substrate surface with the megasonic action applied. Adsorption in this case represents the delivery and noncovalent interactions of the cleaning chemistry with the contaminated substrate needed to effectively enhance particle removal. A second-order kinetic fit (1/{particle count} vs time) was employed for all cleaning chemistries to gain better insight into the synergy between chemistry transport and megasonic action (power).

To better understand the role that megasonic plays in the adsorption kinetics and transport of the SC-1 cleaning chemistry to the wafer surface, the megasonic parameters were explored.

https://doi.org/10.1021/acsomega.2c00683
ACS Omega 2022, 7, 26029−26039

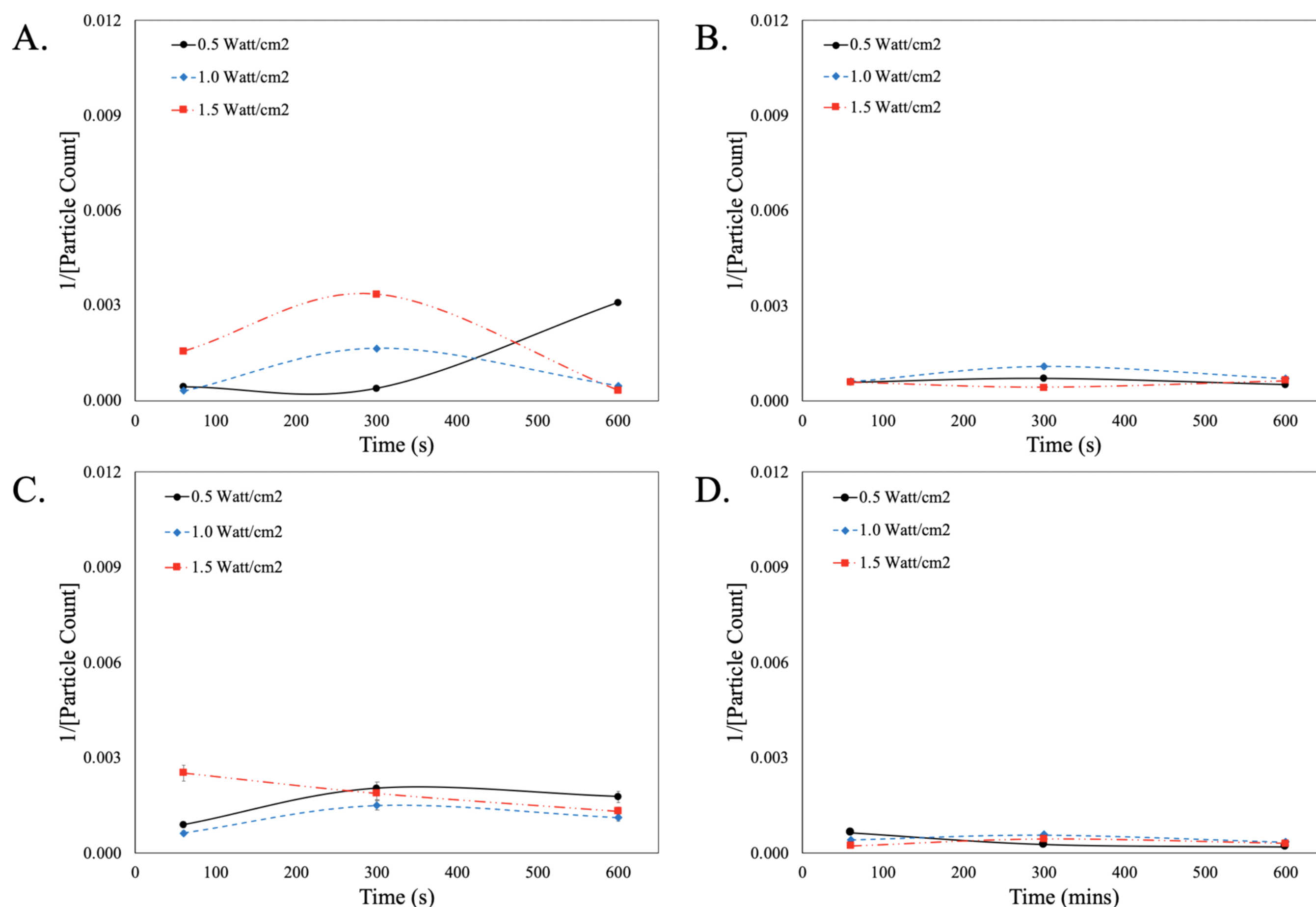

Figure 4. Evaluation of cleaning performance for supramolecular cleaning chemistries using a second-order kinetic model for pulsed-wave megasonic conditions. (A) PE-1198LA, (B) P-103, (C) PSSA, and (D) Tween 20.

Figure 2 is a second-order kinetic model that looks at the cleaning efficiency of SC-1 with continuous megasonic wave and pulsed-wave megasonic conditions. It must be noted that the fit functions presented are not calculated but rather tentative projections for illustrative purposes to guide comparative analysis of cleaning chemistry systems.

When looking at the continuous wave condition, as a function of time the cleaning efficiency increases across all power conditions. This finding validates that for traditional redox chemistries to work effectively, there is a significant buildup time required for the conversion of Ce^{3+} to Ce^{4+}. When comparing the kinetics as a function of power, the low power conditions (i.e., 0.5 and 1.0 W/cm^2) level off at 300 s, indicating that the maximum rate of particle removal is achieved. In the case of the high-power condition (i.e., 1.5 W/cm^2), the rate of particle removal increases linearly as there is a balance between the redox kinetics and the megasonic power. In the case of the pulse kinetics, the lower-power megasonic conditions (i.e., 0.5 and 1.0 W/cm^2) allow for an increase in cleaning efficiency as a function of time. This is due to the pulse of the megasonic action, which allows for the establishment of an effective equilibrium at the surface of the wafer. In the case of the higher-power condition (i.e., 1.5 W/cm^2), the cleaning efficacy is hindered, which can be attributed to a disruption in the generation of ROS, which is necessary for effective redox activity. These findings clearly indicate that when using traditional charge flipping redox chemistries, not only is the transport of the chemistry to the surface crucial but so is balancing the generation of ROS in the system.

As previously mentioned, the aggressive charge flipping that occurs when using the industry standard, SC-1, is not necessarily ideal as severe undercutting may occur. To prevent undercutting, it is proposed that supramolecular cleaning chemistries be used to encapsulate and remove particle contaminants effectively while also preventing further defectivity. Figure 3 surveys supramolecular cleaning chemistries using the second-order kinetic analysis under continuous wave megasonic conditions.

In the case of the anionic micelle (PE-1198LA), the removal of particle contaminants is poor due to the disruption of the micellar network. With the disruption of the micellar network, the mode of particle removal is dependent on the adsorption of the monounits to the particle-coated surface. The strong interaction between the anionic monounit and the positively charged CeO_2 particle coupled with the constant megasonic action disrupts the equilibrium at the surface and therefore prevents its subsequent removal. When looking at the nonionic micelle (P-103) at the low power condition (0.5 W/cm^2) there is a clear indication of time-dependent particle removal. This is because there is time needed to transport the micellar system to the surface and for the micelle to effectively encapsulate rogue particles. Its rate of particle removal then levels off as the megasonic action is not enough to continuously deliver and remove the anionic micellar system from the wafer. When increasing the power to 1.0 W/cm^2, there is a significant increase

https://doi.org/10.1021/acsomega.2c00683
ACS Omega 2022, 7, 26029−26039

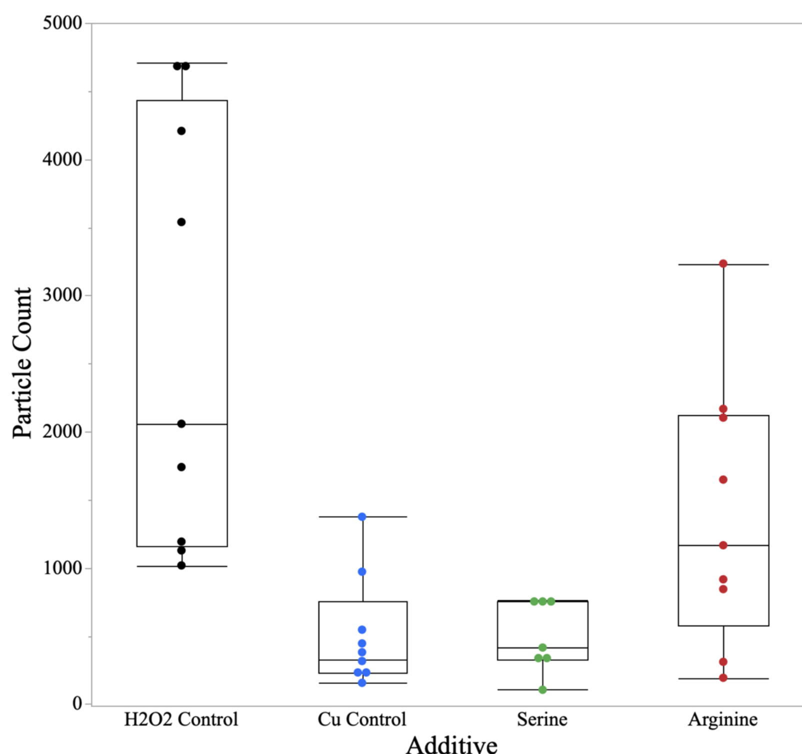

Figure 5. Particle count for ROS-generating species in megasonic cleaning conditions.

in the initial rate of particle removal from the wafer surface due to effective chemistry delivery. However, at the longer times, the cleaning efficiency of P-103 is completely disrupted. Due to the static nature of this megasonic cleaning, this could be an indication of particle redeposition as a function of time. In the case of the anionic polyelectrolyte (PSSA), the cleaning efficacy increases as a function of time which validates the importance of chemistry delivery to the wafer surface. Because of the "fish-net" like network of the polyelectrolyte, the supramolecular structure is not affected by an increase in the megasonic power, which allows for an increase in particle removal. Similar to the polyelectrolyte network, the vesicle (Tween 20) is less likely to break upon exposure to megasonic action. This is seen at the low power conditions (0.5 and 1.0 W/cm^2) removal efficacy is enhanced as a function of time. Similar to that of the micellar networks, there is a buildup time required to get the cleaning chemistry to the wafer surface. In the case of the high-power condition (1.5 W/cm^2) there is a decrease in performance which could be due to subtle disruption in the encapsulation/adsorption equilibrium. With all of these supramolecular chemistries, it is clear that the delivery to the wafer surface and the ability of that supramolecular structure to remain intact and encapsulate particles is critical. To further explore this phenomenon, the second-order kinetic model was employed in the presence of pulsed-wave megasonic conditions. Figure 4 is a summary of the supramolecular cleaning chemistries using a second-order model under pulsed-wave megasonic conditions.

Upon the addition of a pulsed wave to the megasonic cleaning, the performance of the supramolecular cleaning chemistries is completely hindered. This is due to the disruption of the dynamic equilibrium required to effectively remove particles from the surface. In the case of the anionic micelle (PE-1198LA), there is still some performance as the anionic monounit can effectively adsorb to the positively charged CeO_2 surface, resulting in minimal removal.

In the case of SC-1, it was determined that the generation of ROS is crucial to the effective removal of the CeO_2 from the surface of the wafer as it helps convert the surface oxidation state from Ce^{3+} to Ce^{4+}. This conversion in the surface redox state will aid in the weakening of the surface ceria−silanol bond resulting in the effective removal under reduced shear force conditions.[32,33] Therefore, it would be beneficial to take the "soft" cleaning nature of the supramolecular structures and couple them with ROS to maximize particle removal. Specifically, this work will look at incorporating Cu^{2+}−amino acid complexes as they are known to aid in the production of $^{\bullet}OH$ through catalytic Fenton chemistry. Figure 5 is a summary of the particle counts using Cu^{2+}−amino acid complexes under megasonic conditions.

Though the addition of metal−organic complexes may not be optimal for dielectric p-CMP applications, it serves as an excellent model system to validate the impact of ROS on performance. This work focuses on low megasonic power (0.5 W/cm^2) and the shortest time (60 s) to look at the true chemical activity of the system. When looking at the H_2O_2 control, there is a significant amount of variation in particle count as the generation of ROS relies solely on the breakdown of H_2O_2. This process is less controlled than that of the organometallic complexes. In the case of Cu^{2+} only, there is significantly more control in the generation of ROS, which aids in the removal of particles from the wafer surface. For the amino acids in this system, serine and arginine were chosen as they give significantly different $^{\bullet}OH$ generation. As previously mentioned, literature reports that the Cu^{2+}−serine complexes ($\log \beta$ = 14.083)[34] produce 2.00×10^{-14} M of $^{\bullet}OH$, while Cu^{2+}−arginine ($\log \beta$ = 14.007)[34] complexes produce 0.33×10^{-14} M of $^{\bullet}OH$. When looking at the particle counts of these two complexes, it is clear that the generation of $^{\bullet}OH$ significantly aids in the removal of CeO_2 particles. With less production of $^{\bullet}OH$ in the arginine case, there is a significantly higher particle count and variability.

https://doi.org/10.1021/acsomega.2c00683
ACS Omega 2022, 7, 26029−26039

Further exploration of the generation of $^{\bullet}OH$ with ROS species and the subsequent buildup time needed for effective removal was studied using the second-order kinetic model. Figure 6 is a summary of the second-order kinetic model for organometallic complexes at the low megasonic power conditions.

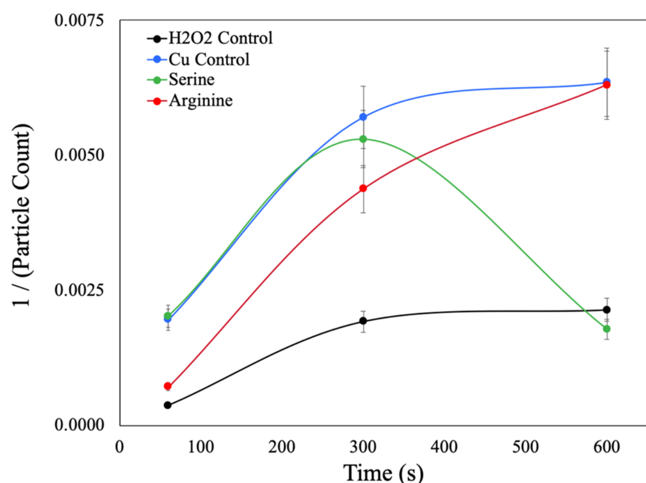

Figure 6. Second-order kinetic model for ROS-generating species in megasonic conditions.

In the case of the H_2O_2-only control, the rate is low in the absence of the organometallic complex catalyst, which is necessary to degrade the H_2O_2 and generate $^{\bullet}OH$. Upon the addition of organometallic complexes, there is a significant increase in the removal of particles from the wafer surface. When looking at the initial rate of particle removal (i.e., 60−300 s), it is clearly seen that Cu^{2+} only and Cu^{2+}−serine complexes show the best performance. Arginine, on the other hand, has a slower rate of particle removal but eventually reaches the same performance as the Cu^{2+} only. This indicates that as a function of time, the Cu^{2+}−arginine complex is disrupted by the megasonic action and the Cu^{2+} in the system dominates. With the Cu^{2+}−serine complexes, the initial rate is fast; however, once all of the excess Cu^{2+} in the system is used, it begins to act like H_2O_2 only. The Cu^{2+}−serine complex is less likely to be broken up by the megasonic action as the binding affinity is stronger than that of Cu^{2+}−arginine.

To further validate the generation of $^{\bullet}OH$ in these Cu^{2+}−amino acid systems, a known UV−vis method and a probe molecule, PNDA, were used. PNDA is known to degrade in the presence of $^{\bullet}OH$; therefore, the λ_{max} at 440 nm can be tracked and correlated back to the generation of $^{\bullet}OH$. It must be noted that work has been done to identify effective probes for the detection of $^{\bullet}OH$ in diverse radical containing/generating environments.[35] Furthermore, Rutely et al.[36] have reported that $^{\bullet}OH$ species generated can in turn react rapidly with H_2O_2 to produce the hydroperoxyl radical ($HO_2^{\bullet}$), which may also have an impact on probe degradation. While the megasonic conditions will generate a diverse population of radicals, the goal of this work was to enhance the surface-active $^{\bullet}OH$ content via catalytic Fenton reactions resulting from organometallic

Figure 7. PNDA degradation in the presence of ROS species. (A) H_2O_2, (B) Cu^{2+} + H_2O_2, (C) Cu^{2+}/serine + H_2O_2, and (D) Cu^{2+}/arginine + H_2O_2.

https://doi.org/10.1021/acsomega.2c00683
ACS Omega 2022, 7, 26029−26039

complexes and H_2O_2. The additional concentration of $^{\bullet}OH$ will further enhance the surface redox reactions required for effective CeO_2 particle removal. Figure 7 is a degradation study of PNDA in the presence of ROS-generating organometallic complexes.

As previously stated, H_2O_2 only does not have a ROS-generating catalyst to help degrade the H_2O_2 into $^{\bullet}OH$. The lack of degradation of PNDA over the course of an hour shows that the oxidizer alone is not sufficient in enhancing the production of $^{\bullet}OH$. This holds true for all three physical conditions, which include a completely static system, a dynamic system mixed with a paddle mixer, and a megasonic condition. In the case of the Cu^{2+} only, there is a steady degradation of PNDA as a function of time but only in the megasonic condition. This indicates that an increase in collisions from the megasonic action is required to aid in the catalytic breakdown of H_2O_2 and in turn degrade PNDA. The high variability of the degradation indicates minimal control over the rate of the catalytic H_2O_2 breakdown. Upon the addition of serine to the system, there is a rapid degradation of the PNDA in the case of sonication and a subtle decay in the static and dynamic cases. This addition of a strong Cu^{2+}−serine complex rapidly degrades the H_2O_2. This rapid degradation further supports the previous data with a drastic drop-off in performance as a function of time. This indicates that the particle removal of Cu^{2+}−serine complexes is only viable for a short period of time. When changing the amino acid in the complex from serine to arginine, the rate of PNDA decay is slower but more controlled. This is because the arginine complex is weak and disrupted by the megasonic action, which then allows the free Cu^{2+} in the system to generate $^{\bullet}OH$ at a controlled rate evident by steady PNDA degradation.

As previously mentioned, coupling these organometallic complexes with supramolecular cleaning chemistries will enhance cleaning efficacy. Moving forward, this work focuses solely on PSSA as the supramolecular cleaning chemistry as its polyelectrolyte network will not be disrupted by the megasonic action. Figure 8 is a summary of the second-order kinetic model for organometallic complexes in the presence of PSSA at the low megasonic power conditions.

One key observation is that the cleaning formulations used in this study have a slow, steady rate of particle removal. This can be attributed to the interactions of chemistries with the PSSA network and the controlled release of the ROS species. In the case of the PSSA + H_2O_2, there is a significant buildup time as the small mobile nature of the H_2O_2 allows for it to be easily released from the polyelectrolyte network. This noncontrolled release allows for a significant increase in ROS generation and particle encapsulation, which in turn enhances particle removal. In the presence of organometallic complexes (i.e., Cu^{2+} only, Cu^{2+}−serine, Cu^{2+}−arginine), there is a significant decrease in particle count when compared to the PSSA-only control. Wherein Cu^{2+} and Cu^{2+}−serine show similar performance as they both have the same ROS generation in the first 600 s. Further validation of this phenomenon is seen with the Cu^{2+}−arginine complex as there is limited ROS generation and only a subtle change in the p-CMP performance.

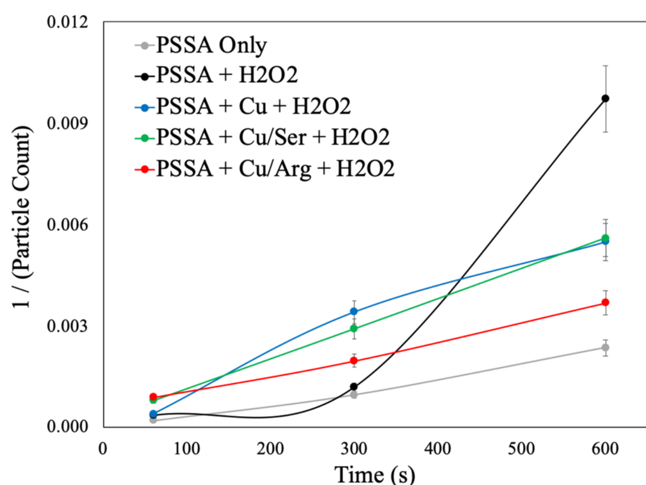

Figure 8. Second-order kinetic model for PSSA with ROS-generating species in megasonic conditions.

To truly understand the synergy occurring between the ROS species and the supramolecular cleaning chemistries, it is crucial to understand the interactions occurring between the two components. Figure 9 surveys the particle count with ROS-generating species in the presence of PSSA.

Though the performance of the Cu^{2+} only and Cu^{2+}−serine complexes is the best for the longer time periods, the Cu^{2+}−arginine complexes show lower particle counts in the first 60 s. This is because the complex between the Cu^{2+} and arginine contains more noncovalent interaction points (six hydrogen bond donors and six hydrogen bond acceptors) than that of the Cu^{2+} and serine complexes (three hydrogen bond donors and four hydrogen bond acceptors). This prevents the complex from entering the cavities of the polyelectrolyte network via noncovalent blocking and therefore can readily generate surface-active $^{\bullet}OH$, which in turn enhances particle removal. Due to its poor ROS-generating capability, the performance does not improve as a function of time. On the other hand, Cu^{2+} only and Cu^{2+}−serine complexes are more likely to fit into the cavities of the polyelectrolyte network. Upon the addition of megasonic action and as a function of time, the organometallic complexes are then released from the matrix. This release from the network then allows for the generation of $^{\bullet}OH$ and for particles to be effectively encapsulated in the PSSA matrix. This is supported by the enhancement of particle removal as a function of time.

To further validate the adsorption phenomena, a modified QCM technique was employed. This technique involved depositing a CeO_2 film on the surface of an Au electrode to simulate a particle-coated wafer surface. The analysis focuses specifically on the instantaneous adsorption of the cleaning chemistries to the CeO_2 surface. Figure 10 outlines the instantaneous rate of adsorption for ROS species with and without the presence of PSSA.

It must be noted that the "without PSSA" control is H_2O and the "with PSSA" control is PSSA alone at the working concentration. Except for the controls, all trials have H_2O_2. When looking at the adsorption of the ROS species to the CeO_2 film, both the Cu^{2+} control and Cu^{2+}−serine show variable adsorption, which can be attributed to the rapid generation of $^{\bullet}OH$. These $^{\bullet}OH$ will interact with the surface of the CeO_2 nanoparticle, which explains the faster rate to reach crystal equilibrium. In the case of the Cu^{2+}−arginine complex, there is only subtle adsorption to the CeO_2 surface as the complex remains in the bulk and there is minimal production of $^{\bullet}OH$ in static conditions. Upon the addition of PSSA to the Cu^{2+}−arginine system, there is no change in the rate of crystal equilibrium. This further validates the finding that the Cu^{2+}−arginine complex does not readily interact with the PSSA matrix and that the production of $^{\bullet}OH$ is slow. When looking at the

https://doi.org/10.1021/acsomega.2c00683
ACS Omega 2022, 7, 26029−26039

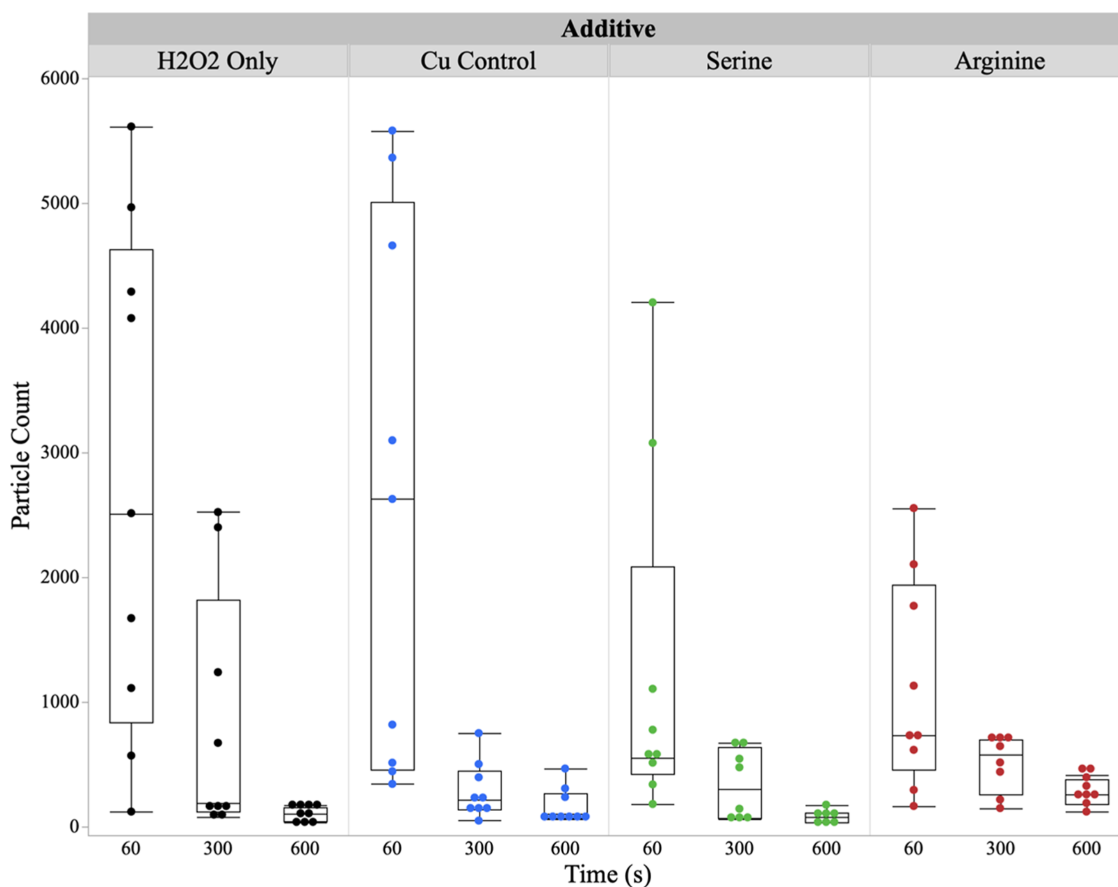

Figure 9. Particle count for PSSA with ROS-generating species in megasonic conditions for (1) H_2O_2 only, (2) H_2O_2 and Cu, (3) H_2O_2, Cu, and serine, and (4) H_2O_2, Cu, and arginine.

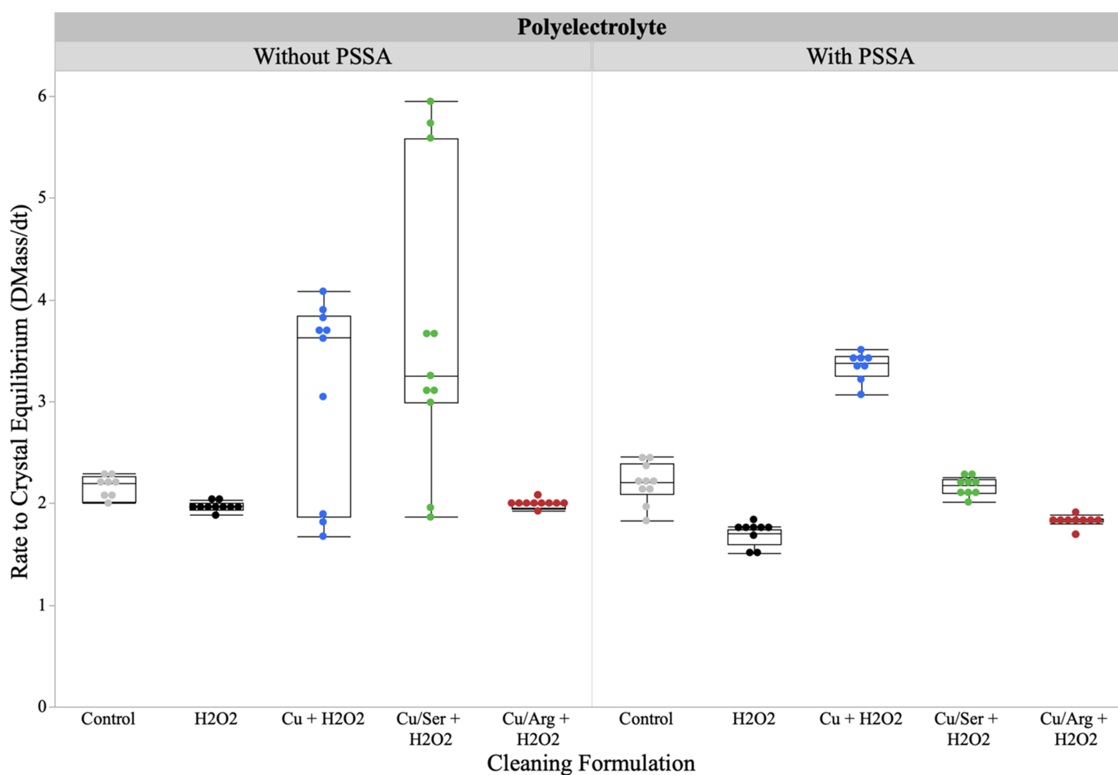

Figure 10. Instantaneous rate of adsorption of ROS species with and without PSSA to a CeO_2 surface.

https://doi.org/10.1021/acsomega.2c00683
ACS Omega 2022, 7, 26029−26039

PSSA-only control and the PSSA + H_2O_2 condition, there is a decrease in the rate of adsorption with H_2O_2. This is due to the oxidative nature of H_2O_2 having the ability to disrupt the electrostatic interaction between the anionic polyelectrolyte and the positively charged CeO_2 surface. Upon the addition of PSSA, the variability of the Cu^{2+} only and Cu^{2+}−serine complexes significantly decreases. This can be attributed to the noncovalent interactions between the PSSA matrix and the organometallic species, which contributes to a more controlled adsorption mechanism. The increase in the rate of adsorption for Cu^{2+} only can be attributed to the ion adsorption to the surface oxygen vacancies of the CeO_2, which in turn enhances the electrostatic attraction of the PSSA matrix. With the Cu^{2+}−serine complex, there will be a high affinity to complex, therefore leaving minimal excess Cu^{2+} ions to interact with the CeO_2 at the surface. As this is an instantaneous rate of adsorption in a static condition, there is a minimal generation of $^{\bullet}$OH to help aid in the adsorption.

4. CONCLUSIONS

This work has demonstrated the importance of the transport of supramolecular cleaning chemistries at the wafer surface on both a macroscopic and molecular level. Specifically, emphasis was placed on coupling supramolecular cleaning chemistries with ROS species and evaluating their performance in the presence of a bench-scale megasonic cleaning process. Results of this coupling show some promise with particle encapsulation but it is highly dependent on the dynamic equilibrium of chemistry to the wafer surface. It was clearly demonstrated the role of ROS species in the efficient conversion of the CeO_2 for noncontact low shear stress removal. Furthermore, coupling supramolecular structures and ROS generators provides similar performance to that of the traditional brush cleaning methods but has significantly reduced particle removal variability. Therefore, this work demonstrated the synergistic balance that exists between the chemical adsorption of the “soft” cleaning chemistries and the cavitation produced during the megasonic cleaning, which is required for optimal performance in particle removal and scratch reduction at low shear force.

AUTHOR INFORMATION

Corresponding Author

Jason J. Keleher − *Department of Chemistry, Lewis University, Romeoville, Illinois 60446, United States;* orcid.org/0000-0003-4310-6094; Email: keleheja@lewisu.edu

Authors

Katherine M. Wortman-Otto − *Department of Chemistry, Lewis University, Romeoville, Illinois 60446, United States;* orcid.org/0000-0003-4905-140X

Don Watson − *ProSys Megasonics, ProSys Inc., Campbell, California 95008, United States*

Don Dussault − *ProSys Megasonics, ProSys Inc., Campbell, California 95008, United States*

Complete contact information is available at: https://pubs.acs.org/10.1021/acsomega.2c00683

Funding

The authors have no outside sources of funding to report for this work.

Notes

The authors declare no competing financial interest.

ACKNOWLEDGMENTS

The authors would like to thank ProSys for their generous donation of the BowlMeg system and their continued collaboration.

REFERENCES

(1) Banerjee, G.; Rhoades, R. L. Chemical Mechanical Planarization Historical Review and Future Direction. *ECS Trans.* **2008**, *13*, 1−19.

(2) Babu, S. *Advances in Chemical Mechanical Planarization (CMP)*; Woodhead Publishing, 2016; pp 1−511.

(3) Patlolla, R. R.; Motoyama, K.; Peethala, B.; Standaert, T.; Canaperi, D.; Saulnier, N. CMP Development for Ru Liner Structures beyond 14nm. *ECS J. Solid State Sci. Technol.* **2018**, *7*, P397−P401.

(4) Srinivasan, R.; Dandu, P. V.; Babu, S. V. Shallow Trench Isolation Chemical Mechanical Planarization: A Review. *ECS J. Solid State Sci. Technol.* **2015**, *4*, P5029−P5039.

(5) Seo, J. A Review on Chemical and Mechanical Phenomena at the Wafer Interface during Chemical Mechanical Planarization. *J. Mater. Res.* **2021**, *36*, 235−257.

(6) Vyas, A. A.; Zhou, C.; Yang, C. Y. On-Chip Interconnect Conductor Materials for End-of-Roadmap Technology Nodes. *IEEE Trans. Nanotechnol.* **2018**, *17*, 4−10.

(7) Sampurno, Y.; Linhart, A. N.; Wortman-Otto, K. M.; Philipossian, A.; Keleher, J. J. Communication—An Analysis of Shear Forces in Post-CMP PVA Brush Scrubbing for Stationary and Rotating Wafers. *ECS J. Solid State Sci. Technol.* **2021**, *10*, No. 034002.

(8) Philipossian, A.; Mustapha, L. Effect of Mechanical Properties of PVA Brush Rollers on Frictional Forces during Post-CMP Scrubbing. *J. Electrochem. Soc.* **2004**, *151*, G632.

(9) Lee, J.-H.; Ryu, H.-Y.; Hwang, J.-K.; Yerriboina, N. P.; Kim, T.-G.; Hamada, S.; Wada, Y.; Hiyama, H.; Park, J.-G. A Breakthrough Method for the Effective Conditioning of PVA Brush Used for Post-CMP Process. *ECS J. Solid State Sci. Technol.* **2019**, *8*, P307−P312.

(10) Keswani, M.; Han, Z. *Post-CMP Cleaning*; Elsevier Inc., 2015; Vol. *VIII*.

(11) Seo, J.; Gowda, A.; Babu, S. V. Almost Complete Removal of Ceria Particles Down to 10 Nm Size from Silicon Dioxide Surfaces. *ECS J. Solid State Sci. Technol.* **2018**, *7*, P243−P252.

(12) Netzband, C. M.; Dunn, K. Investigation into the Effect of CMP Slurry Chemicals on Ceria Abrasive Oxidation State Using XPS. *ECS J. Solid State Sci. Technol.* **2019**, *8*, P629−P633.

(13) Alety, S. R.; V Sagi, K.; Babu, S. V. Role of Ce $^{3+}$ Ions in Achieving High Silicon Nitride Polish Rates. *ECS J. Solid State Sci. Technol.* **2017**, *6*, P898−P903.

(14) Kim, J.; Kim, S.; Paik, U.; Katoh, T.; Park, J. Effect of Crystallinity of Ceria Particles on the PETEOS Removal Rate in Chemical Mechanical Polishing for Shallow Trench Isolation. *J. Korean Phys. Soc.* **2002**, *41*, 413−416.

(15) Wortman-Otto, K. M.; Linhart, A. N.; Dudek, A. L.; Sherry, B. M.; Keleher, J. J. Role of Molecular Structure on Modulating the Interfacial Dynamics for Shallow Trench Isolation (STI) Chemical Mechanical Planarization (CMP) Applications. *ECS J. Solid State Sci. Technol.* **2021**, *10*, No. 024009.

(16) Wu, B.; Wang, P.; Wang, Y.; Qu, X.-P.; Tan, B.; Hamada, S.; Wada, Y.; Hiyama, H. Removal of Nanoceria Abrasive Particles by Using Diluted SC1 and Non-Ionic Surfactant. *ECS J. Solid State Sci. Technol.* **2021**, *10*, No. 034010.

(17) Kwon, T. Y.; Ramachandran, M.; Park, J. G. Scratch Formation and Its Mechanism in Chemical Mechanical Planarization (CMP). *Friction* **2013**, *1*, 279−305.

(18) Choi, J.-G.; Prasad, Y. N.; Kim, I.-K.; Kim, I.-G.; Kim, W.-J.; Busnaina, A. A.; Park, J.-G. Analysis of Scratches Formed on Oxide Surface during Chemical Mechanical Planarization. *J. Electrochem. Soc.* **2010**, *157*, H186.

(19) Wortman-Otto, K. M.; Linhart, A. N.; Mikos, A. M.; Cahue, K. A.; Keleher, J. J. Contact vs. Non-Contact Cleaning: Correlating Interfacial Reaction Mechanisms to Processing Methodologies for

ENHANCED FEOL/BEOL Post-CMP Cleaning. *Solid State Phenom.* **2021**, *314*, 237−246.
(20) Graverson, C. F.; Wortman-Otto, K. M.; Linhart, A. N.; Zubi, T. B.; Keleher, J. J. Development of "Soft" Cleaning Chemistries for Enhanced STI Post-CMP Cleaning. *ECS Trans.* **2019**, *92*, 165−174.
(21) Graverson, C. F.; Wortman-Otto, K. M.; Linhart, A. N.; Sampurno, Y.; Philipossian, A.; Keleher, J. J. Striking a Balance: Role of Supramolecular Assemblies on the Modulation of the Chemical and Mechanical Contributions during Post-STI CMP Cleaning. *Mater. Chem. Phys.* **2021**, *259*, No. 124170.
(22) Brems, S.; Hauptmann, M.; Camerotto, E.; Pacco, A.; Kim, T.-G.; Xu, X.; Wostyn, K.; Mertens, P.; De Gendt, S. Nanoparticle Removal with Megasonics: A Review. *ECS J. Solid State Sci. Technol.* **2014**, *3*, N3010−N3015.
(23) Sahoo, B. N.; Han, S. Y.; Kim, H. T.; Ando, K.; Kim, T. G.; Kang, B. K.; Klipp, A.; Yerriboina, N. P.; Park, J. G. Chemically Controlled Megasonic Cleaning of Patterned Structures Using Solutions with Dissolved Gas and Surfactant. *Ultrason. Sonochem.* **2022**, *82*, No. 105859.
(24) Camerotto, E.; Brems, S.; Haumann, M.; Lurquin, J.; Struyf, H.; Mertens, P. W.; de Gendt, S. Towards an Improved Megasonic Cleaning Process: Influence of Surface Tension on Bubble Activity in Acoustic Fields. *Solid State Phenom.* **2012**, *195*, 173−176.
(25) Cho, S.-H.; Kim, H. J.; Kim, H. Y.; Kim, K. J.; Jeong, H. D. A Study on Scratch Reduction Using the Sonic Dispersion of CMP Slurry. In *Initiatives of Precision Engineering at the Beginning of a Millennium*; Inasaki, I., Ed.; Springer: Boston, MA, 2002. DOI: 10.1007/0-306-47000-4_74.
(26) Cavitation. https://prosysmeg.com/cavitation/.
(27) Acoustic Streaming. https://prosysmeg.com/acoustic-streaming/.
(28) Boundary Layer. https://prosysmeg.com/boundary-layer/.
(29) Chu, C. L.; Lu, T. Y.; Fuh, Y. K. The Suitability of Ultrasonic and Megasonic Cleaning of Nanoscale Patterns in Ammonia Hydroxide Solutions for Particle Removal and Feature Damage. *Semicond. Sci. Technol.* **2020**, *35*, No. 045001.
(30) Balachandran, R.; Deymier, P.; Raghavan, S.; Keswani, M. A Sono-Electrochemical Technique for Enhanced Particle Removal from Tantalum Surfaces. *ECS Solid State Lett.* **2014**, *3*, P49.
(31) Hariharaputhiran, M.; Zhang, J.; Ramarajan, S.; Keleher, J. J.; Li, Y.; Babu, S. V. Hydroxyl Radical Formation in H2O2-Amino Acid Mixtures and Chemical Mechanical Polishing of Copper. *J. Electrochem. Soc.* **2002**, *147*, 3820.
(32) Netzband, C. M.; Dunn, K. Controlling the Cerium Oxidation State During Silicon Oxide CMP to Improve Material Removal Rate and Roughness. *ECS J. Solid State Sci. Technol.* **2020**, *9*, No. 044001.
(33) Wortman-Otto, K. M.; Linhart, A. N.; Dudek, A. L.; Sherry, B. M.; Keleher, J. J. Role of Molecular Structure on Modulating the Interfacial Dynamics for Shallow Trench Isolation (STI) Chemical Mechanical Planarization (CMP) Applications. *ECS J. Solid State Sci. Technol.* **2021**, *10*, No. 024009.
(34) Murphy, J. M.; Powell, B. A.; Brumaghim, J. L. Stability Constants of Bio-Relevant, Redox-Active Metals with Amino Acids: The Challenges of Weakly Binding Ligands. *Coord. Chem. Rev.* **2020**, *412*, No. 213253.
(35) Mortazavian, S.; Bandala, E. R.; Bae, J. H.; Chun, D.; Moon, J. Assessment of P-Nitroso Dimethylaniline (PNDA) Suitability as a Hydroxyl Radical Probe: Investigating Bleaching Mechanism Using Immobilized Zero-Valent Iron Nanoparticles. *Chem. Eng. J.* **2020**, *385*, No. 123748.
(36) Rutely, C. B. C.; Fontmorin, J. M.; Tang Walter, Z.; Xochitl, D. B.; Mika, S. Towards Reliable Quantification of Hydroxyl Radicals in the Fenton Reaction Using Chemical Probes. *RSC Adv.* **2018**, *8*, 5321−5330.

https://doi.org/10.1021/acsomega.2c00683
ACS Omega 2022, 7, 26029−26039